ACS Catalysis

Research Article

pubs.acs.org/acscatalysis

Selective Catalytic Reduction of NO_x of Ship Diesel Engine Exhaust Gas with C_3H_6 over Cu/Y Zeolite

Hesham A. Habib,[†,‡] Ralf Basner,[‡] Ronny Brandenburg,[‡] Udo Armbruster,[†] and Andreas Martin*[,†]

[†]Leibniz-Institut für Katalyse e.V. an der Universität Rostock, Albert-Einstein-Straße 29a, D-18059 Rostock, Germany

[‡]Leibniz-Institut für Plasmaforschung und Technologie e.V., Felix-Hausdorff-Straße 2, D-17489 Greifswald, Germany

Supporting Information

ABSTRACT: Various solid Cu-containing catalysts were prepared. Their performance in the selective catalytic reduction of NO_x using propene as reducing agent from 150 to 450 °C in an O_2-rich model exhaust gas in the presence of water vapor was investigated. This research aimed at the development of a catalytic NO_x to N_2 ($DeNO_x$) step to be part of a ship diesel exhaust abatement system in combination with other techniques, such as nonthermal plasma. Among the catalysts tested, Cu on zeolite Y with an optimized load of 16 wt % (denoted as 16Cu/Y) displayed excellent $DeNO_x$ activity with highest selectivity toward N_2 at 290 °C. The influence of other variables, such as Cu load, calcination temperature, feed composition, and GHSV on the performance of 16Cu/Y was studied, as well. The highest N_2 yield of 98% was achieved using 2000 ppm of propene in the gas feed. The presence of O_2 proved to be a crucial factor for promoting the selective reduction of NO_x with C_3H_6 over this catalyst. On the other hand, the presence of water in the feed decreased NO_x to N_2 conversion. However, the catalyst showed excellent stability over 120 h, even at high water concentration, and also after repeated heating from ambient temperature to 450 °C, and it was reusable after downtimes without remarkable loss in activity. The nature of the Cu species was studied by XPS, XRD, and TPR experiments.

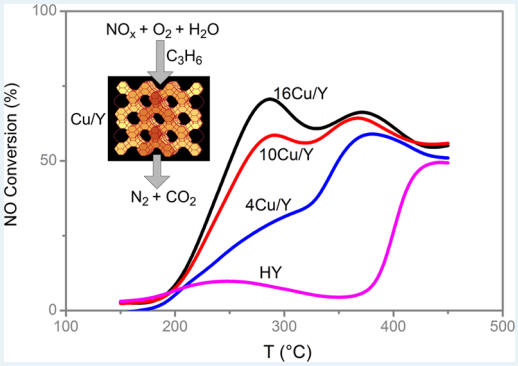

KEYWORDS: *selective catalytic reduction, $DeNO_x$, copper, zeolite, propene*

1. INTRODUCTION

Nitrogen oxides (NO_x) from automobile exhaust gases and industrial combustion of fossil fuels are a major source of air pollution because they cause acid rain, photochemical smog, and ozone depletion.[1−3] Nowadays, marine diesel engines contribute significantly to NO_x emissions. Legislation is expected to set lower NO_x emission limits by 2016, and ship owners will be forced to take measures accordingly.[4] The conversion of NO_x to N_2 ($DeNO_x$) thus is a very important and challenging process in environmental catalysis. Despite the thermodynamic instability of NO and NO_2, the NO_x decomposition is kinetically unfavorable, implying that efficient catalysts are necessary to eliminate NO_x.[5−7] However, in the lean exhaust of fuel-efficient engines (large excess of oxygen), NO_x cannot be reduced efficiently with a conventional three-way catalyst.

There are currently three main alternative catalyst concepts for lean exhaust NO_x reduction: (i) lean NO_x trap (LNT), (ii) ammonia-assisted selective catalytic reduction (NH_3-SCR), and (iii) hydrocarbon-assisted selective catalytic reduction (HC-SCR). LNT catalysts, also known as NO_x storage and reduction catalysts (NSR), generally contain Pt as the active component (e.g., $Pt/BaO/Al_2O_3$) and operate alternatively under lean and rich fuel conditions.[3,8,9] During the lean fuel period, when O_2 is in excess, NO is oxidized into a NO_x mixture (NO + NO_2) over the active Pt centers and is then adsorbed (stored) on Ba surface species as various species (nitrite, nitrate). Before an unacceptable amount of NO_x passes the catalyst due to surface saturation, the motor management switches to rich fuel conditions for a short period during which the stored NO_x is released and reduced into N_2 over Pt.[10] Different types of reducing agents, such as hydrocarbons, CO, and H_2, have been used in NSR catalyst studies,[11] and H_2 has been found to be the most effective. NH_3-SCR takes advantage of the high reduction efficiency of NH_3 and allows continuous operation, and this technology has been developed to market. Although NH_3 effectively reduces NO_x,[12−16] some aspects, such as storage technologies, transportation/leakage, and corrosion, need further improvement. HC-SCR is advantageous with regard to engine integration because hydrocarbons can be easily added to the diesel exhaust by in-cylinder postinjection or in-exhaust secondary injection. Among different hydrocarbons, propene was found to be a good reducing agent for SCR of NO_x.[17−24] Compared with other hydrocarbons; propene might allow extending the operation range to lower temperatures as a result of its higher reactivity. This would make the $DeNO_x$ step more flexible to cope with changing engine loads.

Received: March 17, 2014
Revised: June 16, 2014
Published: June 16, 2014

   dx.doi.org/10.1021/cs500348b | ACS Catal. 2014, 4, 2479−2491

Table 1. Textural Properties of Unsupported Zeolites and the Prepared Supported Cu Catalysts

catalyst	Cu load (wt %)	Cu/Al ratio (mol/mol)	BET surface area (m^2/g)	av pore diameter (nm)	total pore vol (cm^3/g)	micropore vol (cm^3/g)	micropore area (m^2/g)
NH_4–Y[a]			950.9	1.7	0.41	0.34	888
H–Y[b]			521	1.7	0.22	0.18	473
4Cu/Y	4.06	0.19	679	1.7	0.30	0.25	647
10Cu/Y	9.75	0.43	667	1.7	0.33	0.29	652
16Cu/Y	15.89	0.72	686	1.6	0.29	0.25	660
H-ZSM-5[a]			409	3.6	0.37	0.11	253
19Cu/ZSM-5	18.52	2.65	328	4.1	0.37	0.08	175
NH_4-MOR[a]			508	2.9	0.23	0.19	485
19Cu/MOR	19.42	2.44	417	2.3	0.24	0.14	346
H-Beta[a]			623	4.8	0.39	0.29	586
19Cu/Beta	19.10	2.48	482	2.5	0.30	0.15	340

[a]Si/Al ratio of parent NH_4–Y = 2.3 (calculated from elemental analysis data); SiO_2/Al_2O_3 ratios of parent H-ZSM-5 = 34.0, NH_4-MOR = 20.5, H-Beta = 25.0–60.0, respectively (supplied from Zeochem AG and ZEOLYST C.V.). [b]H–Y is the calcination product of NH_4–Y at 400 °C/3 h.

Noble metals supported on oxides have already been commercialized as three-way catalysts; however, the scarcity and relatively high price of noble metals (e.g., Pt, Rh, Pd) limit their practical application. Various oxide supports, such as ZrO_2 and Al_2O_3, which were promoted by Co, Ni, etc., have been studied for $DeNO_x$ with hydrocarbons.[25−27] However, many of these catalysts deactivate in the presence of water vapor.[28] Beyond that, zeolite-based catalysts such as ZSM-5, Y, and Beta types have received attention for applicability in HC-SCR of NO_x as a result of their high activity within a wide temperature window.[29−31] In expensive transition metals (e.g., Fe, Co, Cu) embedded in a zeolite matrix show higher catalytic activity and selectivity in $DeNO_x$ than the parent zeolites.[32−34]

The first catalyst that was found to have a good hydrocarbon-assisted NO_x reduction capability under oxygen-rich conditions was Cu/ZSM-5.[35,36] In recent years, Cu-zeolite catalysts have been extensively studied for the $DeNO_x$ reaction because of their low cost, durability, and low-temperature activity.[37−46] Catalysts containing highly dispersed CuO on a variety of supports have demonstrated competitive levels of activity, stability, and durability under simulated operating conditions.[47] There is evidence that isolated copper ions are the active sites for the HC-SCR, and small CuO crystallites can accelerate the direct oxidation of hydrocarbons.[44,48] Moreover, because of the interaction between the supports and the active metal species, the properties of the active components often differ from those of the corresponding bulk metal oxides. Therefore, the catalytic properties of the active copper phase can be greatly influenced by the dispersion of copper species and the nature of the support.[49,50] However, because a large amount of water vapor is present in engine exhaust, its effect on the catalyst activity must be taken into account. Cu-ZSM-5, which is the most extensively studied catalyst for the SCR of NO_x by hydrocarbons, suffers from rapid and severe deactivation by exposure to a low concentration of water vapor.[51]

The present work describes results from a project entitled "Plasma-based catalytic treatment of exhaust emissions of marine diesel engines", which is a part of the international research program MARTEC ERA-NET.[52] It addresses novel plasma-based catalytic technologies for the reduction of pollution from marine shipping diesel engines and involves developing a demonstration reactor to operate in the real exhaust gas from a ship's diesel engine (Sulzer 6A20/24 driven with ultralow sulfur diesel of 0.001% sulfur). Together with the introduction of sulfur emission control areas (SECAs) by the International Maritime Organization of the United Nations,[4] the tendency worldwide goes to lower the sulfur content of the marine fuels, and therefore, SO_2 was excluded in the studies described here. Such nonthermal plasma technologies in direct combination with a unique catalyst will be investigated to reveal new technology for future exhaust treatment. The typical operation conditions of low-speed marine diesel engines is lower (below 400 °C) than for automotive engines (500–600 °C). This lowers the hydrothermal stress on solid catalysts.

Recent studies proved that the maximum of NO oxidation efficiency by means of plasma treatment of the exhaust gas is independent of the NO/NO_2 ratio, and up to 55% of the NO was oxidized to mainly NO_2.[53,54] The effect of plasma treatment (i.e., the energy consumption for $NO–NO_2$ conversion) was significantly improved by the addition of propene because additional oxidizing radicals are generated. Since the effect of plasma at relevant energy needs is somewhat restricted to NO to NO_2 oxidation and additional process for NO_2-removal is needed. The aim of the present work was to investigate a catalytic process utilizing propene as the reducing agent that can be combined with plasma activity in a subsequent step. Therefore, a series of Cu/Y catalysts with various Cu loadings were prepared and evaluated in the selective catalytic reduction of a model off-gas containing NO_x, water vapor, and O_2 in excess from 150 to 450 °C with propene as reducing agent.

The effect of catalyst features (Cu loading and calcination temperature) and reaction conditions (concentration of NO_x, O_2, H_2O, C_3H_6 in the feed; GHSV) on the NO_x reduction were investigated thoroughly. With regard to application and, in particular, to resistance to changing reaction conditions, the long-term stability of the best-performing catalyst was investigated, and various engine loads were simulated. Nitrogen physical sorption (BET), elemental analysis (ICP-OES), temperature-programmed reduction (TPR), X-ray diffraction (XRD), and X-ray photoelectron spectroscopy (XPS) were employed to characterize the prepared catalysts. The catalysts are planned to be finally supported on macroscopic structures such as ceramic honeycombs or metal grids for applications in abatement of NO_x in ship diesel exhausts.

2. EXPERIMENTAL SECTION

2.1. Catalyst Preparation. The Cu/Y zeolite catalysts were prepared by incipient wetness impregnation of a zeolite Y in ammonium form (Sigma-Aldrich, Si/Al molar ratio = 2.3) with

dx.doi.org/10.1021/cs500348b | ACS Catal. 2014, 4, 2479−2491

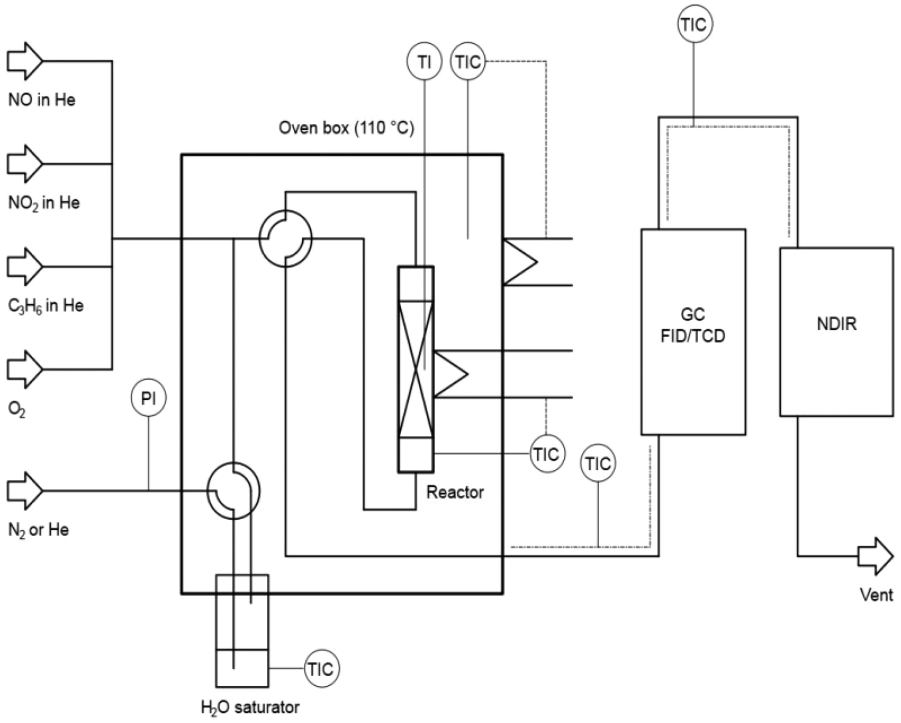

Figure 1. Flow scheme of the continuous setup.

an aqueous solution of $Cu(NO_3)_2{\cdot}3H_2O$. The amount of solution and concentration of Cu were appropriately chosen to achieve a complete wetness of the zeolite powder. The samples were dried at 120 °C overnight, followed by calcination at 400 °C in a muffle under air for 2 h. Discussed samples will be designated as *x*Cu/Y where *x* represents the copper content as weight percent (exact values as determined by ICP-OES are listed in Table 1). Other zeolites, such as H-Beta (ZEOCAT PB) and H-ZSM-5 (ZEOCAT PZ-2/25), were supplied from Zeochem AG (Uetikon), whereas mordenite NH_4-MOR (CBV 20A) was supplied by ZEOLYST C.V. Cu-containing catalysts based on these zeolites are denoted in the same way as described above for Cu/Y solids.

To realize a first application test with a real diesel engine, a lot of 10 kg of a calcined 16Cu/Y catalyst powder was prepared. In a second step, this material was mixed in an aqueous slurry with an ethanolic solution of a suited binder (hydroxypropylcellullose, MW 100 000 Da) and then impregnated onto 24 commercial monoliths (porous cordierite (Rauschert Veilsdorf GmbH, Germany), 150 × 150 × 150 mm^3). The entire honeycomb body has 41 × 41 channels, and each channel has a square cross section of 3.2 × 3.2 mm^2.

2.2. Catalyst Characterization Methods. N_2-adsorption capacities, calculated as specific surface areas, cumulative pore volumes, average pore diameters, micropore volumes, and micropore areas of the catalysts and supports were determined by N_2 sorption at −196 °C on a Micromeritics ASAP 2010C analyzer. Samples were degassed at 400 °C for 3 h under vacuum before measurement.

The X-ray diffraction measurements were carried out on a STADI P automated transmission diffractometer (STOE Darmstadt, Germany) using Cu $K\alpha_1$ radiation (λ = 0.15406 nm) and a 6° linear position-sensitive detector. The alignment was checked by use of a silicon standard. The data were collected in the 2θ range from 5 to 70° with a step size of 0.5° and 50 s measurement time per step. The phase composition of the samples was determined using the program suite WINXPow by STOE with inclusion of the Powder Diffraction File PDF2 of the ICDD (International Centre of Diffraction Data).

The H_2-TPR experiments were performed using a home-made gas flow system, including a fixed-bed quartz reactor and a gas analyzer unit. Optimum sample weights for the chosen reduction conditions were estimated according to the equation by Monti and Baiker.[55] Hydrogen consumption was monitored by a calibrated thermal conductivity detector (GOW-MAC Instruments), and the peak areas were integrated for quantitative analysis.[56] Before analysis, the samples were heated in a synthetic air flow (50 mL/min) from 25 to 400 °C (rate = 2 K/min; final hold, 2 h), followed by cooling to 50 °C in a dry nitrogen flow. The experiment comprised two reduction steps with an intermediate reoxidation. First, TPR was carried out with 5.15% of H_2 in Ar (15 mL/min) at a heating rate of 10 K/min to 550 °C, then a reoxidation step with 10 vol % of N_2O in He (30 mL/min) over 30 min at 50 °C was appended to oxidize Cu^0 to Cu^{1+} at mild conditions. Afterward, the TPR procedure was repeated (oxidized surface TPR, denoted as s-TPR[57]) to reduce Cu^{1+} back to Cu^0.

The XPS measurements were performed with a VG Escalab 220iXL (ThermoFisher) using Al Kα radiation (E = 1486.6 eV). The spectra were referred to the C 1s peak at 284.8 eV. The electron binding energies and the peak areas were determined by fitting the peaks with Gaussian−Lorentzian curves using the program suite Unifit 2010. The concentrations of the elements in the near-surface region were obtained after division by the element-specific Scofield factors and the transmission function of the spectrometer.

2.3. Catalyst Testing. The evaluation of various catalysts in selective catalytic reduction of NO_x by propene was performed continuously at atmospheric pressure in a fixed-bed quartz microreactor (Figure 1) with an inner diameter of 6 mm. Typically, 0.1 g (0.15 cm^3) of catalyst (0.315−0.710 mm) was

dx.doi.org/10.1021/cs500348b | ACS Catal. 2014, 4, 2479−2491

placed in the reactor and pretreated with the reaction feed gas at 150 °C for 30 min. In the first stage of this study, a short-time test protocol was applied to test several catalysts and to elucidate the impact of important reaction parameters. The catalyst performance was studied between 150 and 450 °C at a rate of 2 K/min, which means that the catalyst was in nonsteady operation mode. In such a standard test, the nominal feed gas composition is as follows: 1000 ppm of NO_x, 1000 ppm of C_3H_6, 12% of O_2, 5% of H_2O, and He as the balance. Because of the inlet temperature and chemical equilibrium, part of the NO was converted into NO_2 prior to entering the reactor, and therefore, the feed typically contained 850 ppm of NO and 90 ppm of NO_2. This was considered when calculating conversion and yield. Water was added to the feed by passing helium through a saturator with deionized water at known temperature. The flows were controlled by mass flow meters (MKS). In all the tests (except studies on the GHSV effect), the total feed flow rate was 120 mL/min, corresponding to a space velocity of ~47 000 h^{-1}. Continuous analysis of NO and NO_2 was accomplished by a three-channel multigas sensor (Limas 11HW, ABB, Germany). Simultaneously, additional online analyses were made using a gas chromatograph (HP 6890) equipped with a TCD detector (sampling interval 10 min). A molecular sieve 5A capillary column served for the separation of H_2, N_2, O_2, and a Porapak Q capillary column for analysis of N_2O, CO_2, and C_3H_6. Conversions of NO, NO_x, and C_3H_6 as well as the N_2 yield were calculated as follows:

$$X(\mathrm{NO}) = ([\mathrm{NO}]_{\mathrm{inlet}} - [\mathrm{NO}]_{\mathrm{outlet}})/[\mathrm{NO}]_{\mathrm{inlet}} \times 100\% \quad (1)$$

$$X(\mathrm{NO}_x) = ([\mathrm{NO}_x]_{\mathrm{inlet}} - [\mathrm{NO}_x]_{\mathrm{outlet}})/[\mathrm{NO}_x]_{\mathrm{inlet}} \times 100\% \quad (2)$$

$$X(\mathrm{C_3H_6}) = ([\mathrm{C_3H_6}]_{\mathrm{inlet}} - [\mathrm{C_3H_6}]_{\mathrm{outlet}})/[\mathrm{C_3H_6}]_{\mathrm{inlet}} \times 100\% \quad (3)$$

$$Y(\mathrm{N_2}) = 0.5 \times [\mathrm{N_2}]/[\mathrm{NO}]_{\mathrm{inlet}} \times 100\% \quad (4)$$

Conversion of NO passes a maximum with temperature as a result of limitation by available C_3H_6 amount. The corresponding temperature is further labeled as T_{max}. The formation of N_2O was found to be negligible (<10 ppm) at any temperature, and for this reason, this product will not be further discussed in the present study. Blank experiments were performed with the empty reactor and did not show any measurable NO_x reduction in the investigated temperature range. Similarly, no significant C_3H_6 oxidation was observed below 350 °C. Tests by replacing helium with N_2 as the balance proved that NO_x formation from N_2 (as present in real off-gas) could be excluded in the presence of catalysts at chosen conditions.

3. RESULTS AND DISCUSSION

3.1. Characteristics of the Prepared Cu/Y Catalysts.

3.1.1. N_2 Sorption. The textural properties of the solid samples are summarized in Table 1. N_2 sorption isotherms are of type I, according to IUPAC nomenclature, confirming the microporous nature of all the samples.[58] The calculated specific BET surface areas and the pore volumes decreased by adding Cu to the NH_4-Y support. Calcination of NH_4-Y forms HY and produces acid sites, and simultaneously, the BET surface area drops. Rehydration of H-Y inevitably leads to partial disruption of the framework, which might be reduced by the introduction of copper.

On the other hand, no significant difference in the surface areas of the Cu/Y catalysts can be observed. The data confirmed that the sorption capacities of the zeolites did not change with different Cu loadings, and therefore, no extensive pore plugging or deterioration of the zeolite Y structure had occurred during sample preparation, which is also demonstrated by the XRD patterns (section 3.1.2). The catalysts prepared from other zeolites, that is, 19Cu/ZSM-5, 19Cu/MOR, and 19Cu/Beta, possessed significantly lower surface areas (328−482 m^2/g) as well as larger pore diameters (2.3−4.1 nm) compared with Cu/Y samples (1.6−1.7 nm).

3.1.2. X-ray Diffraction. Crystallinity and phase composition of the NH_4-Y zeolite and the Cu-containing catalysts made thereof were analyzed by XRD, and the diffraction patterns are shown in Figure 2. The relative intensities of reflections change

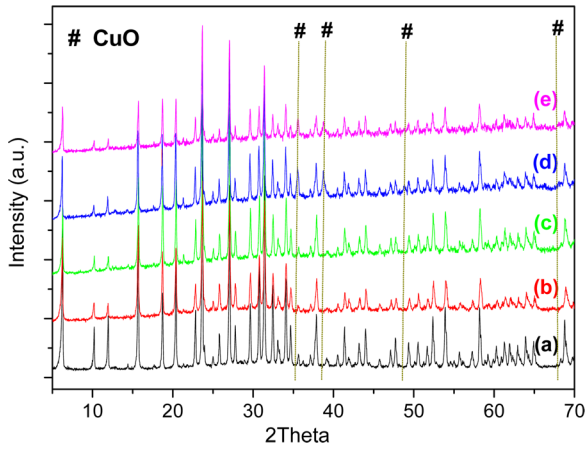

Figure 2. XRD patterns of (a) NH_4-Y, (b) 4Cu/Y, (c) 10Cu/Y, (d) 16Cu/Y and (e) spent 16Cu/Y.

due to the amount of Cu loading on the catalyst surface. Two intense reflections corresponding to CuO (2θ = 35.3°, 38.6°) are clearly visible for the 16Cu/Y catalyst, which is in agreement with the XPS results (section 3.1.4). The absence of these reflections in 10Cu/Y and 4Cu/Y catalysts points to the formation of finely dispersed CuO species on the zeolite supports that cannot be detected by this technique. At the same time, no reflections pointing to Cu_2O species were observed in all the Cu/Y catalysts studied. Most important, the phase composition of the 16Cu/Y catalyst did not change after use in $DeNO_x$ reaction, indicating that the catalyst structure is stable under these conditions. In addition, a more in-depth investigation of the XRD patterns of fresh and spent 16Cu/Y samples shows a slight decrease in the sample crystallinity; however, the intensities of CuO reflections in both samples are more or less equal. Metallic Cu was not detected by XRD in the fresh and spent samples.

3.1.3. Temperature-Programmed Reduction. The reducibility of Cu^{2+} is a function of both the nature of the support and the dispersion of the active phase and is linked to several reduction steps (eqs 5−7):

$$\mathrm{Cu_2O + H_2 \rightarrow 2Cu + H_2O} \quad (5)$$

$$\mathrm{CuO + H_2 \rightarrow Cu + H_2O} \quad (6)$$

$$\mathrm{2CuO + H_2 \rightarrow Cu_2O + H_2O} \quad (7)$$

dx.doi.org/10.1021/cs500348b | ACS Catal. 2014, 4, 2479−2491

The theoretical amount of H_2 consumption expected for a complete reduction of Cu^{2+} to metallic Cu^0 ($n - m = 2$) or to Cu^+ ($n - m = 1$) can be calculated according to eq 8:

$$Cu^{n+} + (n - m)/2H_2 \leftrightarrow Cu^{m+} + (n - m)H^+, \quad \text{with } 0 \leq n \leq m \tag{8}$$

The calcined 16Cu/Y sample showed a change in oxidation state, $n - m = 1.33$ (atom ratio H/Cu), calculated from Table 2

Table 2. Quantitative TPR Results Obtained on (*x*)Cu/Y and (*x*)Cu/Y-(act.) Catalysts

measurement	parameter	4Cu/Y	10Cu/Y	16Cu/Y
ICP analysis	Cu fraction in calcined sample (wt %)	4.06	9.75	15.80
	specific Cu content (mmol/g)	0.64	1.53	2.49
TPR	H_2 consumption (mmol/g) (h_1)	0.3	0.633	1.652
s-TPR	H_2 consumption (mmol/g)	0.03	0.04	0.09
	exposed surface Cu^0 (mmol/g)[a]	0.06	0.08	0.18
TPR-(Ar)	H_2 consumption (mmol/g) (h_2)	0.3	0.497	1.154
s-TPR-(Ar)	H_2 consumption (mmol H_2/g)	0.03	n.d.[d]	0.11
	exposed surface Cu^0 (mmol/g)[a]	0.06	n.d.[d]	0.22
evaluation	portion of weakly stabilized $Cu^{2+} = (h_1 - h_2)/h_1$	0	0.215	0.301
	H_2 (mmol/g) consumed by Cu^{2+} to Cu^0 [b]	0.639	1.535	2.488
	H_2 (mmol/g) consumed by Cu^{2+} to Cu^+ [c]	0.320	0.768	1.244

[a]According to reaction (5). [b]According to reaction (6). [c]According to reaction (7). [d]Not determined.

during first TPR, pointing at the formation of Cu^+/Cu^0. Therefore, mostly Cu^{2+} and Cu^+ were present in the original calcined sample.[59] The reduction depth was less pronounced for 4Cu/Y and 10Cu/Y ($n - m = 0.94$ and 0.82). Obviously the catalyst reducibility increased with Cu loading, which might help to improve the $DeNO_x$ activity (section 3.2).

The catalyst 4Cu/Y exhibited a single reduction peak at 335 °C (T_{max} in NO_x reduction = 330 °C; section 3.2.4). By increasing the Cu content to 16 wt %, two new reduction peaks below 300 °C (T_{max} in NO_x reduction = 290 °C; section 3.2.4) and a shoulder around 335 °C appeared. According to the literature,[60] the reduction peaks in this low-temperature range can be assigned to the Cu^{2+}-to-Cu^+ reduction step (eq 7). The reduction peaks at 335 °C could be assigned to the reduction of Cu^{2+} to Cu^+ inside supercages of faujasite zeolites, whereas those below 300 °C represent the reduction of Cu^{2+} to Cu^+ inside sodalite cages. In addition, the s-TPR results for the three catalysts revealed only small amounts of Cu^0 (Table 2, entry 3).

To show the importance of O_2 for the pretreatment at 600 °C on the redox behavior of such Cu catalysts, the TPR profiles were compared with that of a separate pretreatment experiment using Ar (denominated as TPR-(Ar)). The H_2 consumption during TPR of Cu/Y and Cu/Y-(Ar) samples in dependence on the Cu content is shown in Table 2. After Ar pretreatment, the H_2 consumption of all Cu/Y samples showed smaller $n - m$ values around 1. Such pretreatment conditions are less suited for preparation of catalysts for $DeNO_x$.

3.1.4. X-ray Photoelectron Spectroscopy. To identify the Cu species on the surface of the Cu-exchanged zeolites, the catalysts were studied by XPS (Figure 3). The spectra of all the Cu/Y catalysts showed main signals at 932–933 and 952–953

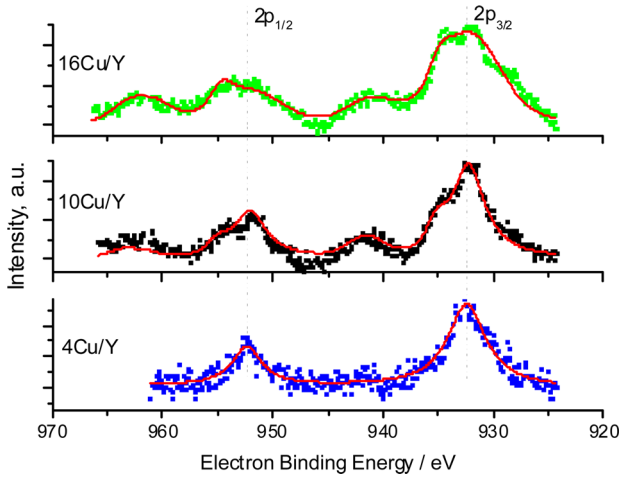

Figure 3. XP spectra of fresh 4Cu/Y, 10Cu/Y, and 16Cu/Y catalysts.

eV, which were assigned to Cu $2p_{3/2}$ and Cu $2p_{1/2}$ states, respectively. In general, they might be related to Cu^{2+} species. For the 10Cu/Y and 16Cu/Y samples with high Cu load, additional satellite signals at 941 and 962 eV evidence the presence of CuO. Furthermore, the main Cu $2p_{3/2}$ and Cu $2p_{1/2}$ signals of the 10Cu/Y and 16Cu/Y samples can be deconvoluted into two signals, which are assigned to the presence of two different Cu^{2+} species. The Cu $2p_{3/2}$ signal revealed two peaks at 932.5 eV (~85%) and 935.3 eV (~15%) for 16Cu/Y and at 932.5 eV (~90%) and 935.6 eV (~10%) for 10Cu/Y catalyst. The more intense signal can be assigned to CuO, and the smaller shoulderlike signal points, to intracrystalline Cu^{2+} species existing as a result of Cu^{2+} coordination to surface oxygen atoms in the structure of the zeolites.[61,62] In addition, the shoulderlike smaller peaks in the Cu $2p_{3/2}$ and Cu $2p_{1/2}$ main signals recorded for 10Cu/Y and 16Cu/Y were observed at slightly higher binding energies than that typical for CuO (933.8 and 953.7 eV),[63,64] which might be attributed to the effect of the zeolite framework.[65] This finding is in agreement with the XRD data for 16Cu/Y showing CuO signals. However, no such CuO reflections were found for 10Cu/Y, because very small particles cannot be detected by XRD. The absence of the satellites in the XP spectrum of 4Cu/Y indicates the absence of CuO species;.[66,67] however, there can be some CuO, but it could not be detected either by XRD or by XPS; probably there is some X-ray amorphous CuO in deeper layers. Therefore, the peak in the spectrum of the 4Cu/Y sample might be due to the presence of intracrystalline Cu^{2+} species only. Other Cu species like Cu^+ or Cu^0 were not detected.

The XP spectra of the spent 16Cu/Y catalysts show the same main features as the fresh ones, with some slight differences (SI, Figure S1). The main Cu $2p_{1/2}$ and Cu $2p_{3/2}$ signals were observed at nearly the same binding energy as in the fresh one. The recorded shift by 2–3 eV indicates structural changes rather than the formation of new Cu^{2+} species. The shoulders in these signals vanished almost completely, whereas the satellite signals seem to be more intensive than in the fresh sample, suggesting that CuO species are now predominant. In contrast to that, XPS data for the spent sample 10Cu/Y still reveal the presence of probably intraframework Cu^{2+} species

dx.doi.org/10.1021/cs500348b | ACS Catal. 2014, 4, 2479–2491

along with CuO. Obviously, the higher the Cu load in the catalyst, the easier CuO species can form. Such formation of CuO might be linked to the increase in the average oxidation state of the working catalyst, most likely by NO_2, which is the stronger oxidant.

3.2. Activity Tests. The main goal of the SCR reaction is the reduction of NO_x toward N_2 in the presence of excess O_2, accompanied by simultaneous oxidation of the reducing agent. The following reactions contribute to the overall process:[68]

$$NO + C_3H_6 + 4O_2 \rightarrow 0.5N_2 + 3CO_2 + 3H_2O \quad (9)$$

$$2NO + C_3H_6 + 4O_2 \rightarrow N_2O + 3CO_2 + 3H_2O \quad (10)$$

$$C_3H_6 + 4.5O_2 \rightarrow 3CO_2 + 3H_2O \quad (11)$$

NO can be reduced completely to N_2 (eq 9) or reacts partly toward N_2O (eq 10). The latter can be neglected in our reaction system because N_2O concentrations were less than 10 ppm.

3.2.1. Catalyst Efficiency. With 16Cu/Y catalyst in excess of O_2, propene was oxidized to CO_2 (eq 11), and no other oxygenates were detected via GC. Figure 4a,b shows the

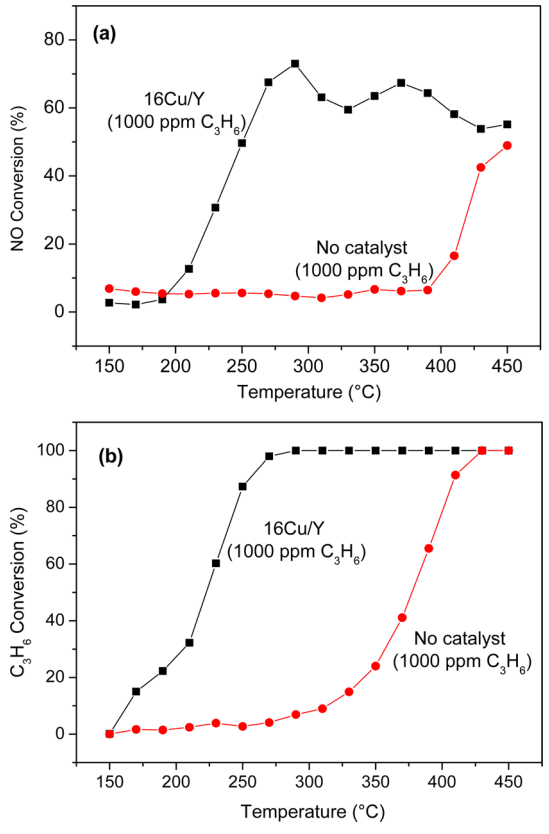

Figure 4. Effect of 16Cu/Y catalyst on the conversions of NO (a) and C_3H_6 (b) (1000 ppm of NO_x, 1000 ppm of C_3H_6, 12 vol % O_2, 5 vol % H_2O, He as balance, 0.1 g catalyst, GHSV = 47 000 h^{-1}).

conversions of NO and propene in the presence and absence of 16Cu/Y catalyst, respectively. In the blank experiment with 1000 ppm of NO_x, 1000 ppm of propene, H_2O, and excess O_2 without catalyst, NO and C_3H_6 were poorly converted below 350 °C. In the presence of 16Cu/Y, the ignition point for propene oxidation was around 150 °C, whereas no remarkable NO_x conversion was observed below 200 °C. Regarding the possible role of intermediates from propene oxidation in NO_x conversion, the observed sequence in activation of reactants on this catalyst would be beneficial because NO_x conversion at low temperatures is not limited by availability of reducing species. The catalyst extends the operation range for oxidation of NO to NO_2 down to 200 °C, where no homogeneous reaction takes place.

The maximum NO conversion of 73% was reached at 290 °C, corresponding to 100% C_3H_6 oxidation. At higher temperatures (330–350 °C), the NO conversion decreased as a result of the complete consumption of C_3H_6 as the rate of concurrent deep oxidation (eq 11) increased with temperature at the cost of NO reduction.

Figure 5 illustrates that 16Cu/Y was also able to convert NO_2 immediately to N_2 with very high selectivity, even under

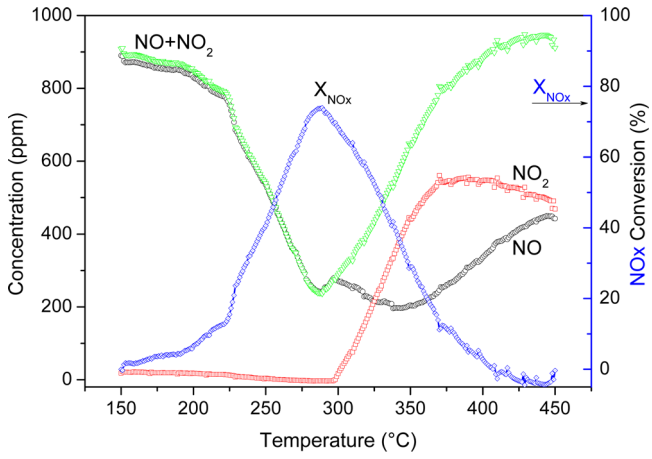

Figure 5. Effect of temperature on the NO_x concentrations and conversion over 16Cu/Y (1000 ppm of NO_x, 1000 ppm of C_3H_6, 12 vol % O_2, 5 vol % H_2O, He as balance, 0.1 g catalyst, GHSV = 47 000 h^{-1}).

O_2 excess. In the optimum temperature range, around 290 °C (lowest NO concentration), a sharp decrease in the total NO_x concentration by 73% comes along with the formation of N_2, as proved by simultaneous GC analysis.

With further temperature increase, the rate of C_3H_6 oxidation seemed to outnumber NO oxidation and consecutive NO_2 decomposition rates, and because no C_3H_6 was left, the concentration of NO_x fell back to inlet concentration. However, as a result of thermodynamic equilibrium, the ratio of NO and NO_2 was then close to equity.

3.2.2. Effect of Support Nature on NO_x Reduction over Different Cu Zeolites. Figure 6 illustrates the performance of catalysts with 16 wt % Cu loading supported on different zeolites in C_3H_6-SCR. All catalysts show a first maximum in NO to N_2 conversion at 270–310 °C. A second local maximum in NO conversion due to the formation of NO_2 by homogeneous reaction, which sometimes exceeded the first one, was observed at 370–390 °C. According to the applied temperature program with a continuous heating rate from 150 to 450 °C, the data were collected at nonsteady operation mode. Thus, reported temperature data for maximum conversions may include a slight temperature offset. Simultaneously, NO_x may be converted into nitrites and nitrates on the catalyst surface,[8−10] and such effects may pretend NO conversion until surface saturation is reached. Additional experiments proved that such a storage effect was partly reversible on Cu zeolites because a temperature increase first

dx.doi.org/10.1021/cs500348b | ACS Catal. 2014, 4, 2479−2491

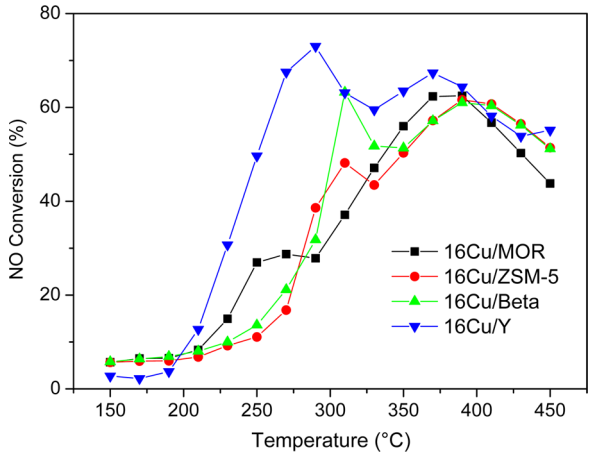

Figure 6. Effect of support on NO conversion over different Cu zeolites with 16 wt % load (1000 ppm of NO_x, 1000 ppm of C_3H_6, 12 vol % O_2, 5 vol % H_2O, He as balance, 0.1 g catalyst, GHSV = 47 000 h^{-1}).

led to a strong release of NO_2 until a new equilibrium was established. These effects were not relevant in long-term runs (section 3.2.9); however, the described test procedure was suitable for providing quick and meaningful data, allowing evaluation of catalyst performance in $DeNO_x$ reaction and influence of reaction parameters.

Among all catalysts studied, 16Cu/Y showed the highest activity at the lowest T_{max}. The order of activities in T_{max} was 16Cu/Y > 19Cu/Beta > 19Cu/ZSM-5 > 19Cu/MOR (Table 3). The catalyst activity seems to correlate with the specific

Table 3. Performance of 16Cu/Zeolites in C_3H_6-SCR at T_{max}

catalyst	Cu load (wt %)	N_2 yield (%) (T_{max})	NO conversion (%) (T_{max})
16Cu/Y	15.89	73.0 (290 °C)	67.3 (370 °C)
19Cu/Beta	19.10	63.2 (310 °C)	61.0 (390 °C)
19Cu/ZSM-5	18.52	48.2 (310 °C)	61.6 (390 °C)
19Cu/MOR	19.42	28.7 (270 °C)	62.4 (370 °C)

BET surface areas rather than with the metal load (see below). Deeper analysis shows that although the Cu load and, thus, the specific number of Cu atoms per surface area is lowest for 16Cu/Y, this catalyst is the most active one. As a result of these observations, more intensive studies on the best performing 16Cu/Y catalyst were carried out.

3.2.3. Effect of Calcination Temperature on the Activity of 16Cu/Y Catalyst. All catalysts described above were routinely calcined at 400 °C. Because the 16Cu/Y catalyst showed the highest activity, another two samples of the precursor were submitted to calcination at 550 and 750 °C and afterward evaluated in C_3H_6-SCR. No remarkable loss in the maximum NO conversion (~70%) was observed, and T_{max} remained unchanged (Figure 7). As proved by XRD analyses (not depicted), the 16Cu/Y catalyst did not undergo severe structural changes up to 750 °C, and optimum activity was preserved. These results demonstrate that this catalyst possesses high strength against thermal stress and that it is not necessary to calcine the precursor far above the reaction temperature.

3.2.4. Effect of Cu Loading on NO_x Reduction. Without Cu loading, the calcined form of the NH_4-Y zeolite support showed negligible activity in C_3H_6-SCR below 350 °C. The effects of

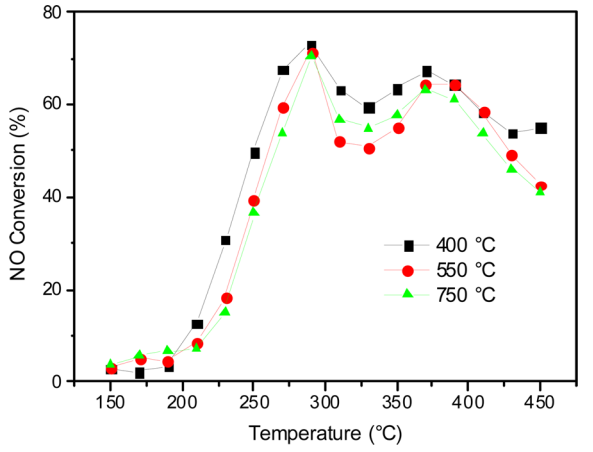

Figure 7. Effect of calcination temperature on activity of 16Cu/Y catalyst in C_3H_6-SCR (1000 ppm of NO_x, 1000 ppm of C_3H_6, 12 vol % O_2, 5 vol % H_2O, He as balance, 0.1 g catalyst, GHSV = 47 000 h^{-1}).

Cu loadings of 4, 10, and 16 wt % with increasing reaction temperature on NO conversion compared with the blank support are shown in Figure 8a. All catalysts were highly active, and the Cu sites on the catalyst surface are definitely essential for NO conversion. The Cu/Y catalysts with lower loadings needed a higher temperature to reach significant NO conversion. With an increase in the Cu loading from 4 to 10

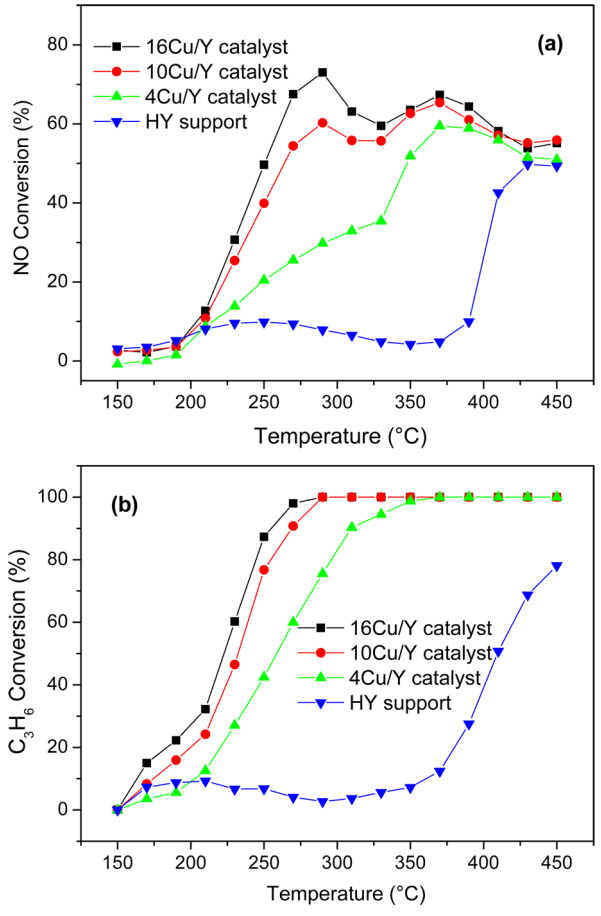

Figure 8. Effect of Cu loading on the conversions of NO (a) and C_3H_6 (b) over Cu/Y catalysts (1000 ppm of NO_x, 1000 ppm of C_3H_6, 12 vol % O_2, 5 vol % H_2O, He as balance, 0.1 g catalyst, GHSV = 47 000 h^{-1}).

dx.doi.org/10.1021/cs500348b | ACS Catal. 2014, 4, 2479−2491

and 16 wt %, the conversion of NO to N_2 was improved from 35% to 60% and 73% at corresponding T_{max}'s. Simultaneously, the T_{max} of NO reduction and the temperature to reach 100% C_3H_6 conversion shifted from 330 to 290 °C and from 350 to 290 °C, respectively (Figure 8b). Obviously the catalytic activity for this reaction depends not only on the catalyst BET surface area (see above), but also on the copper loading, that is, the amount of easily reducible Cu^{2+}/Cu^{+} species (see TPR results). As a reference, different Cu/Y samples were prepared; calcined under argon; and finally, tested for DeNO$_x$ efficiency. No reduction was observed for such systems, confirming that Cu^{2+} species such as CuO are most likely the active sites in the catalytic removal of NO via formation of NO_2.

3.2.5. Effect of C_3H_6 Inlet Concentration on NO_x Reduction over Cu/Y Zeolites. The effect of C_3H_6 on the performance of the described three Cu/Y catalysts was studied with concentrations of 1000, 1500, and 2000 ppm, while all other conditions were fixed: 1000 ppm of NO_x, 12 vol % of O_2, 5 vol % of H_2O in helium as balance at GHSV = 47 000 h^{-1}. The N_2 yield increased steadily upon raising the C_3H_6 feed concentration over all the Cu catalysts (Figure 9). For the 16Cu/Y

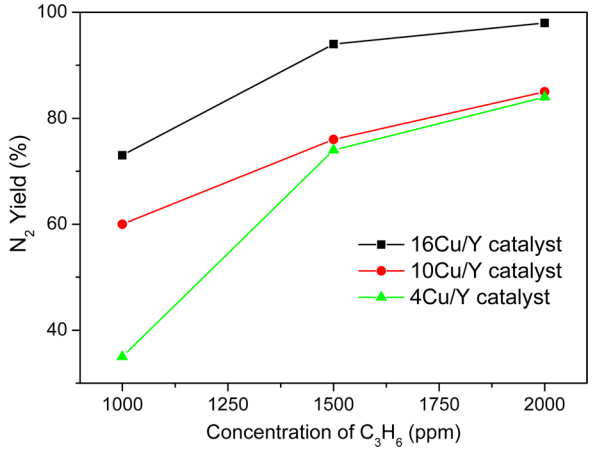

Figure 9. Effect of C_3H_6 concentration on the performance of different Cu/Y systems (1000 ppm of NO_x, 1000−2000 ppm of C_3H_6, 12 vol % O_2, 5 vol % H_2O, He as balance, T_{max} = 290−330 °C, 0.1 g catalyst, GHSV = 47 000 h^{-1}).

catalyst, the maximum N_2 yield increased from 73% to 98% when the C_3H_6/NO_x ratio was doubled. On the other hand, maximum N_2 yields of 85% and 84% were observed when using 2000 ppm of C_3H_6 for 10Cu/Y and 4Cu/Y catalysts, respectively. The complete oxidation of 2000 ppm of C_3H_6 was achieved at 310 °C, whereas that of 1500 ppm of C_3H_6 was accomplished at 290 °C. Higher concentration of reducing agent is beneficial to the reduction of NO_x, which is in agreement with previous research[69−71] showing that increasing the amount of C_3H_6 enhances the formation of intermediate $C_xH_yO_z$ species and thereby facilitating NO_x reduction. Another likely explanation is the formation of reduced sites on the catalyst surface that promote reduction. However, the process has to be optimized with regard to NO_x destruction efficiency and C_3H_6 costs as well as possible release of the latter to the ambient in case of incomplete conversion (depending on engine performance).

3.2.6. Effect of O_2 Concentration on NO_x Reduction over 16Cu/Y Catalyst. Several studies of NO_x conversion with zeolite-based catalysts indicated that the reaction mechanism proceeds via the oxidation of NO to NO_2.[72,73] If the availability of O_2 limits the NO_2 production, this will influence the activity for overall NO_x reduction. This was studied with the 16Cu/Y catalyst, starting with a blank experiment (Figure 10a,b). The

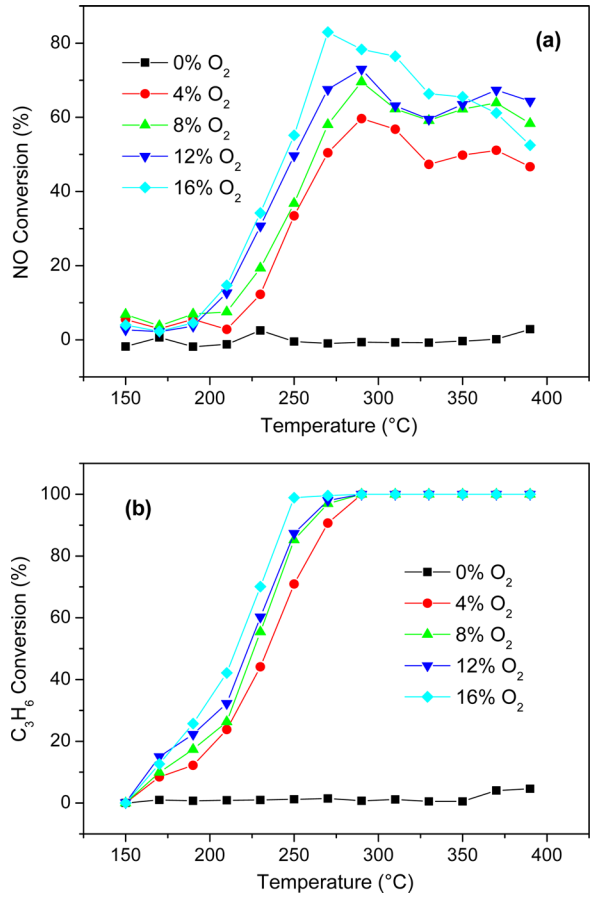

Figure 10. Effect of O_2 concentration on NO conversion (a) and C_3H_6 oxidation (b) over 16Cu/Y (1000 ppm of NO_x, 1000 ppm of C_3H_6, 0−16 vol % O_2, 5 vol % H_2O, He as balance, 0.1 g catalyst, GHSV = 47 000 h^{-1}).

run in the absence of O_2 demonstrated that the NO + C_3H_6 reaction did not start below 450 °C. On the other hand, by introducing 4% of O_2 to the feed, the conversions of C_3H_6 and NO_x increased sharply around 150 and 200 °C, respectively. By increasing the O_2 concentration stepwise, the NO conversion improved significantly to 60% (4% O_2), 69% (8% O_2), 73% (12% O_2), and 83% (16% O_2), whereas the temperature T_{max} slightly shifted from 290 to 270 °C. The temperature to reach maximum conversion of C_3H_6 also shifted toward lower values (250 °C).

3.2.7. Effect of H_2O Concentration on NO_x Reduction over 16Cu/Y Catalyst. All runs discussed so far were carried out with 5 vol % of water in the feed up to 450 °C reaction temperature, which is a typical value for lean-burn marine diesel engine exhaust. In addition to temperature, hydrothermal stability is probably the most crucial factor for catalyst lifetime. We additionally tested our 16Cu/Y catalyst from 600 to 800 °C in the presence of 10% steam over 20 h, and we observed catalyst destruction first above 700 °C. This is indicated by XRD data, as documented in the Supporting Information (SI, Figure S2).

Figure 11 shows the influence of the H_2O concentration on NO conversion over the 16Cu/Y catalyst. A maximum

dx.doi.org/10.1021/cs500348b | ACS Catal. 2014, 4, 2479−2491

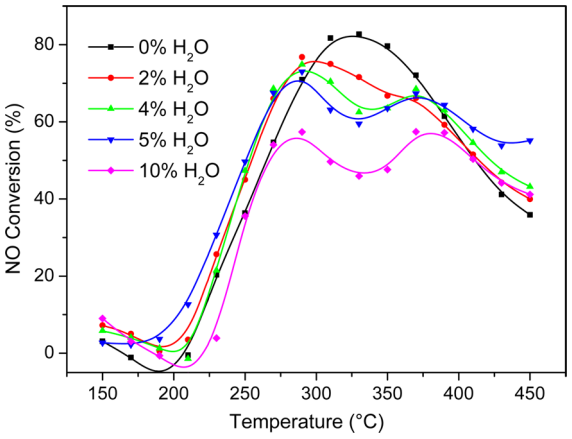

Figure 11. Effect of water vapor concentration on the conversions of NO over 16Cu/Y catalyst (1000 ppm of NO_x, 1000 ppm of C_3H_6, 12 vol % O_2, 0−10 vol % H_2O, He as balance, 0.1 g catalyst, GHSV = 47 000 h^{-1}).

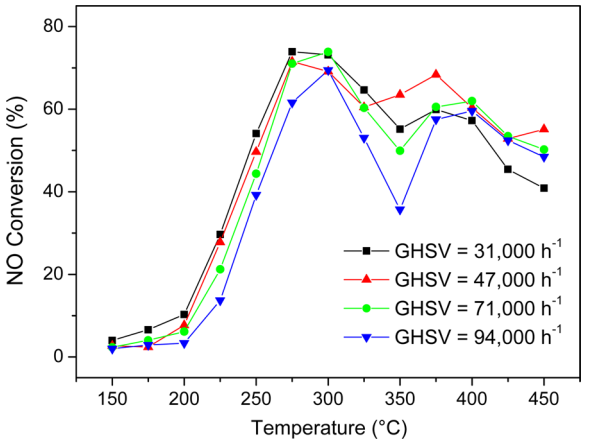

Figure 12. Effect of GHSV on the conversion of NO over 16Cu/Y catalyst (1000 ppm of NO_x, 1000 ppm of C_3H_6, 12 vol % O_2, 5 vol % H_2O, He as balance, 0.1 g catalyst, GHSV = 31 000−94 000 h^{-1}).

conversion of 83% was achieved in the absence of water vapor (corresponding to an 83% N_2 yield). By raising the H_2O content to 10 vol %, NO conversion decreased to 56%, and the temperature, T_{max}, shifted by ∼40 K to lower values. This inhibition effect is attributed to H_2O molecules' blocking the active NO oxidation sites.[74,75] Simultaneously, the onset of C_3H_6 oxidation was shifted to higher temperatures (not depicted), probably as a result of fewer available active sites and less formed NO_2, which might react with C_3H_6 consecutively. Thus, higher temperature (around 270 °C) was required to convert propene completely at the given GHSV. At higher temperature, conversion of NO toward NO_2 was ruled by equilibrium, as described above (see section 3.2.1).

It is remarkable that in the absence of water, only one broad maximum in NO conversion around 325 °C was visible. In all other runs, the addition of water lowered the NO conversion, but because no propene was available above 270 °C, the remaining NO could react toward only NO_2, following the concentration course as described above (see Figure 5), finally forming two maxima.

3.2.8. Effect of GHSV on NO_x Reduction over 16Cu/Y Catalyst. The temperature-programmed tests of 16Cu/Y at GHSV values from 31 000 to 71 000 h^{-1} resulted in NO conversions of 70−75% at T_{max} = 290 °C. By increasing space velocity to 94 000 h^{-1}, the maximum NO_x conversion was decreased by 5%, and T_{max} shifted slightly to a higher temperature (Figure 12). In addition, C_3H_6 conversion decreased strongly with increasing GHSV, and T_{max} shifted slightly, by 25 K, to a higher temperature (not depicted). Complete conversion of C_3H_6 was reached at 300−350 °C. A further increase in the GHSV to 236 000 h^{-1} (not depicted) led to a sharp decrease in conversion of NO_x to N_2, to 44%, with a shifting of T_{max} to a higher temperature of 315 °C. These observations suggest that the 16Cu/Y catalyst is effective in NO_x removal over a wide range of GHSV, which is beneficial with regard to changing engine loads and flow rates.

3.2.9. Effect of Engine Load on Catalyst Performance. In real SCR systems, the inlet conditions strongly depend on the engine load, which sets the temperature and composition of the off-gas. Thus, modifying the total NO_x content and the NO/NO_2 ratio in model gas mixtures is a good way to simulate changes in the engine load at realistic operation conditions. Consequently, standard tests were made with an overall NO_x concentration of 1000 ppm, representing ∼50% engine load. A series of independent tests was carried out with NO_2/NO_x inlet ratios between 0 and 1 while the total concentration of inlet NO_x was kept at 1000 ppm (Table 4). To approach realistic conditions, N_2 served as a balance instead of He.

Table 4. Composition of Feeds with Various Ratios of NO and NO_2[a] and Corresponding NO Conversion at 290 °C[b]

	actual values				
	NO/NO_2 (ppm)		NO_2/NO_x		
set point; NO/NO_2 (ppm)	off[c]	on[d]	off[c]	on[d]	X_{NO} at 290 °C (%)
1000:0	860:85	908:22	0.09	0.02	58
750:250	716:293	760:90	0.29	0.11	65
500:500	400:525	660:213	0.57	0.24	61
250:750	205:745	545:340	0.78	0.38	55
0:1000	6:960	428:458	0.99	0.52	52

[a]At a fixed nominal NO_x concentration of 1000 ppm). [b]12 vol % O_2, 5 vol % H_2O, 1000 ppm propene, balance N_2; 100 mg of catalyst; GHSV 47 000 h^{-1}. [c]Reactor off. [d]Reactor on after 30 min.

Figures 13 and 14 show the course of NO and NO_x conversions from 150 to 450 °C for various NO_2 fractions in the feed (expressed as NO_2/NO_x ratio) at a simulated engine load of 50%. The inlet concentrations of NO and NO_2, which were initially measured at ambient temperature, deviated slightly from the set points (Table 4, reactor off), as a result of chemical equilibrium between NO and NO_2. After heating the reactor to 150 °C, new concentrations were established (Table 4, reactor on). Because of the presence of the catalyst, NO/NO_2 equilibrium was established quickly; however, it was without decomposition to N_2. For example, the NO_2/NO_x ratio dropped from 99 to 52%. With all chosen feed compositions, NO inlet concentration then amounted to at least 400 ppm. During these first stages from ambient temperature to 150 °C, the catalyst most likely adsorbed part of the NO and NO_2 to form surface intermediates (storage effect). Therefore, the system was held for 30 min at 150 °C to establish equilibrium saturation on the catalyst surface, which has to be considered when interpreting the conversion and selectivity data in the following.

dx.doi.org/10.1021/cs500348b | ACS Catal. 2014, 4, 2479−2491

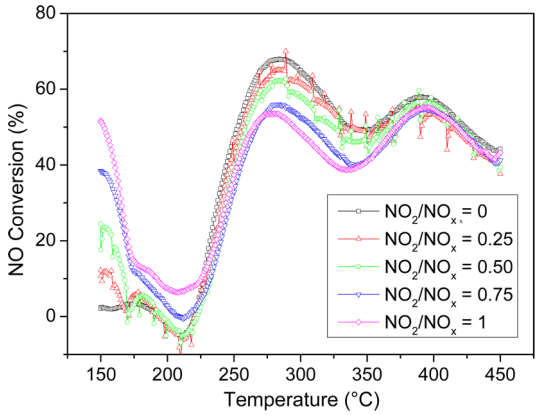

Figure 13. NO conversion at different NO/NO_2 ratios (expressed as NO_2/NO_x) over 16Cu/Y from 150 to 450 °C (1000 ppm of NO_x, 1000 ppm of C_3H_6, 12 vol % O_2, 5 vol % H_2O, N_2 as balance, 0.1 g catalyst, GHSV = 47 000 h^{-1}).

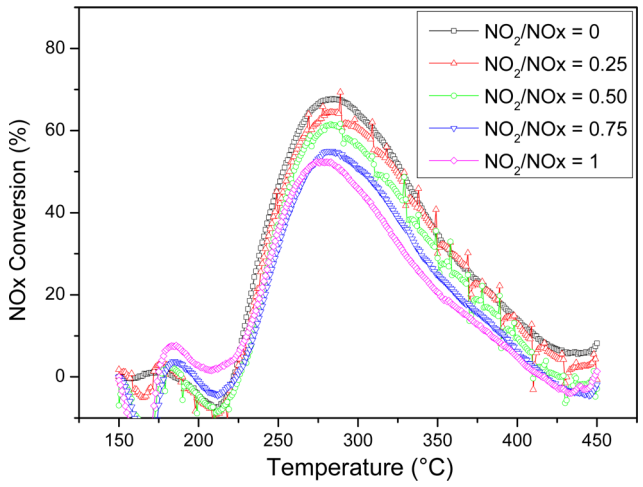

Figure 14. NO_x conversion at different NO/NO_2 ratios (expressed as NO_2/NO_x) over 16Cu/Y from 150 to 450 °C (1000 ppm of NO_x, 1000 ppm of C_3H_6, 12 vol % O_2, 5 vol % H_2O, N_2 as balance, 0.1 g catalyst, GHSV = 47 000 h^{-1}).

After this hold period, the conversion of NO_x was close to zero (see Figure 13). When the temperature was increased slowly, part of the adsorbed NO_x desorbed from the catalyst, pretending negative conversion at first. When the temperature reached the ignition point for NO_x conversion at 220 °C, a sharp increase in the NO_x conversion to more than 50% at a T_{max} of 250−270 °C, depending on feed composition, was observed.

Surprisingly, the higher the initial NO_2 concentration, the lower the final NO_x conversion to N_2 at T_{max} (see Figure 14). Possibly, both compounds compete for adsorption sites on the catalyst surface and the NO oxidation would be hampered as a result of lower surface coverage. In addition, it was suggested that NO_2 is a strong oxidizing agent that could oxidize the metal sites and prevent O_2 from adsorbing and reacting on the surface.[76] A high NO_2 concentration thus would suppress the NO oxidation, which is the O_2-consuming step. A similar NO_2 inhibition effect on the NO oxidation reaction has been reported on various other catalysts.[77,78]

The highest NO/NO_2 feed ratio led to 68% NO and 67% NO_x conversion, whereas the lowest ratio allowed only 53% NO and 52% NO_2 conversion. The similar conversions indicate that the equilibrium does not rule the overall rate. Upon further temperature increase, the NO conversion decreased until the second maximum around 380 °C (see Figure 13), which is attributed to a homogeneous shift of the NO/NO_2 equilibrium (section 3.2.1).

3.2.10. Reusability and Long-Term Stability of 16Cu/Y Catalyst. The frequently alternating charge state of automotive engines affects the composition, temperature, and space velocity of exhaust gases, and this may strongly shorten the catalyst lifetime as a result of thermal stress and structural changes. To assess the reusability and long-term stability of the 16Cu/Y catalyst, two different series of experiments were made:

In the first test, the same lot of 16Cu/Y was used in five subsequent standard runs under the same conditions, following the usual temperature program from 150 to 450 °C with a rate of 2 K/min. Figure 15 depicts the NO_x conversions and the N_2

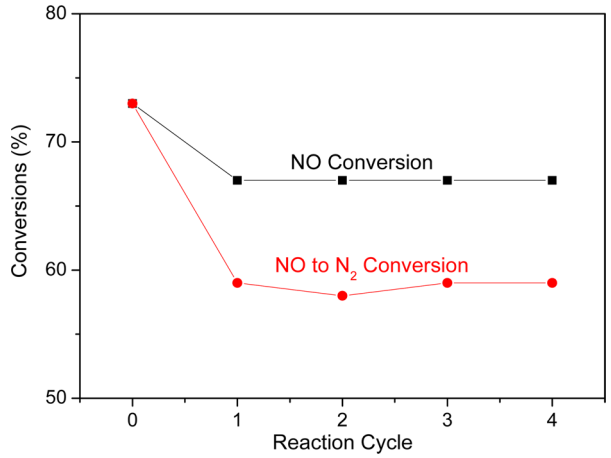

Figure 15. Activity of 16Cu/Y catalyst at 290 °C in five subsequent runs (1000 ppm of NO_x, 1000 ppm of C_3H_6, 12 vol % O_2, 5 vol % H_2O, He as balance, 0.1 g catalyst, GHSV = 47,000 h^{-1}).

yields that were measured at 290 °C. The catalyst lost ∼5% in NO_x conversion after the first run; however, all the following tests showed 68% conversion without further deactivation. The initial activity loss came along with a 14% decrease in the N_2 yield, reaching a stable value of 60% (corresponding to a N_2 selectivity of 88%).

In the second test, the catalytic activity was tested for 120 h at the optimum $DeNO_x$ temperature of 290 °C with the same feed gas composition. This temperature corresponds to the maximum in NO_x reduction under standard test conditions (nominal 1000 ppm of propene, 5 vol % of H_2O, GHSV 47 000 h^{-1}). Figure 16 shows no appreciable deactivation after 120 h on-stream. Furthermore, a stable N_2 yield of 41% was recorded over the complete run time. It implies that 16Cu/Y catalyst has the potential for future application.

3.2.11. Immobilization of 16Cu/Y on monoliths and up-scaling. As reported above, 16Cu/Y-loaded monoliths were manufactured by a slurry technique. After calcination at 700 °C, the mass fraction of active compound as balanced typically amounted to ∼9 wt %. These monoliths were placed in a reactor module, which was directly connected to a commercial marine diesel engine (Sulzer 6A20/24 drive). Figure 17 depicts the performance of this catalyst in $DeNO_x$ of the related off-gas, with a total flow of 150 m^3/h containing 1500 ppm of propene, for three set points at engine loads of 10, 30, and 35%,

dx.doi.org/10.1021/cs500348b | ACS Catal. 2014, 4, 2479−2491

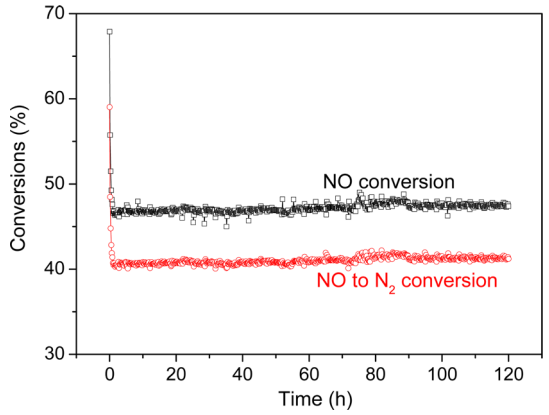

Figure 16. Long-term test with 16Cu/Y at 290 °C (1000 ppm of NO_x, 1000 ppm of C_3H_6, 12 vol % O_2, 5 vol % H_2O, He as balance, 0.1 g catalyst, GHSV = 47 000 h^{-1}).

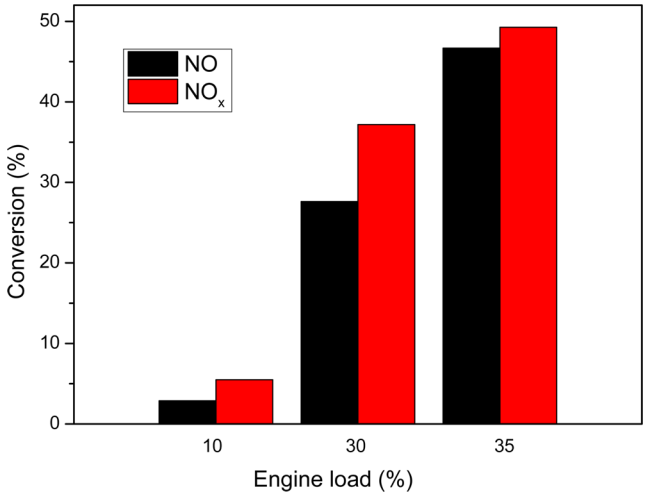

Figure 17. Results from a pilot-scale test with 16Cu/Y immobilized on commercial monoliths at different engine loads.

corresponding to off-gas temperatures of 195, 270, and 290 °C, respectively. It clearly demonstrates that the lab-scale results were nearly reproduced and that this catalyst shows high potential for technical application. Further investigations, also by combining plasma treatment to such a system, are currently running.

4. CONCLUSIONS

In this study, a series of copper-exchanged zeolites has been prepared and investigated for the SCR of NO_x by C_3H_6 in the presence of excess O_2 and high water vapor content for marine diesel exhaust cleaning. The $DeNO_x$ efficiencies of different supported Cu catalysts were significantly affected by the zeolite structure as well as the Cu content. Among these catalysts, Cu/Y catalysts allowed the highest conversion of NO_x to N_2 (98%) and simultaneously shifted the optimum temperature to lower values of around 290 °C. The better performance of Cu/Y systems compared with catalysts derived from other zeolite supports depended on the amount of easily reducible Cu^{2+} species. The fraction of these species increased significantly with an increase in the copper loading from 4 to 16 wt %, as observed by XRD, TPR, and XPS investigations of the 16Cu/Y sample. It appears that the catalyst that is first above a specified minimum Cu load is able to provide such Cu species that are needed for simultaneous oxidation and reduction.

The presence of O_2 and a reducing agent at the same time is crucial for an optimal performance of Cu/Y catalysts in NO_x removal. Increasing the O_2 concentration allowed the effective initial oxidation of NO to intermediate NO_2 and significantly promoted the C_3H_6-SCR of NO_x. In the same manner, the higher the concentration of reducing agent propene, the higher the N_2 yield (up to 98%). It is remarkable that the 16Cu/Y shows the capability to catalyze oxidation and reduction at the same time, and the reaction rates are well balanced to obtain high overall $DeNO_x$ rates. Adding water vapor to the feed decreased the catalyst activity because active $DeNO_x$ sites may get blocked; however, this effect was completely reversible by lowering the water concentration in the feed.

Our results demonstrated the high tolerance of the 16Cu/Y catalyst against variation of the most important reaction parameters (feed composition, GHSV). In particular, 16Cu/Y proved to be stable even after treatment at 750 °C and reusable after downtimes and repeated temperature-programmed operation from ambient to 450 °C. This is very important with regard to its use in a real $DeNO_x$ reactor, which is required to operate with high efficiency at frequently changing reaction conditions due to actual engine load.

It is very promising for application of this catalyst that a first long-term test at optimum conditions revealed high stability against hydrothermal stress. The 16Cu/Y catalyst showed a stable NO conversion of 47% at 290 °C over 120 h without interruption. Hence, the present work provides, for the first time, a detailed parameter study aimed at the potential application of Cu/Y catalyst systems in C_3H_6-SCR of NO_x under lean exhaust conditions (a large excess of O_2) in the presence of water vapor for marine diesel exhaust cleaning. The optimum temperature with propene as the reducing agent was established at around 290 °C. Typical low-speed diesel engines operate with exhaust temperatures below 300 °C, and recent low-speed engines with remarkable performance levels have exhaust temperatures below 250 °C. The obtained results are encouraging concerning combining such a single-reactor $DeNO_x$ step as an integral part of a diesel exhaust treatment system with desulfurization units and other technologies, for example, low-temperature plasma treatment, to be installed on naval vessels. However, for real application, the propene costs compared with other reducing agents have to be considered. Otherwise, propene could be more easily handled compared with liquid ammonia on board such vessels.

The mechanism and reaction network of the $DeNO_x$ reaction over such catalysts is extremely complex. The Cu/Y catalyst has some very special features that definitely need deeper investigation and subsequent optimization. For further optimization and evaluation of such catalysts, more sophisticated measurement methods are currently being developed in our group to get reliable kinetic data and to take into account storage effects on the catalyst surface as well as the contribution of homogeneous reactions of NO and NO_2 under given conditions. Finally, the potential of 16Cu/Y has to be tested with real diesel engine off-gas. Preliminary tests already have demonstrated the feasibility of covering ceramic honeycomb structures with 16Cu/Y catalyst without losing catalyst activity.

dx.doi.org/10.1021/cs500348b | ACS Catal. 2014, 4, 2479−2491

■ ASSOCIATED CONTENT

Supporting Information

XP spectra of spent 10Cu/Y and 16Cu/Y catalysts (Figure S1a), comparison of XP spectra of fresh 4Cu/Y, 10Cu/Y, 16Cu/Y and spent 10Cu/Y, 16Cu/Y catalysts (Figure S1b), XRD patterns of (a) fresh 16Cu/Y, (b) 16CuY (600 °C/10% steam/20h), 16CuY (700 °C/10% steam/20h) and 16CuY (800 °C/10% steam/20h) (Figure S2a), comparison of XRD patterns of (a) NH_4−Y, (b) 4Cu/Y, (c) 10Cu/Y, (d) 16Cu/Y, (e) spent 16Cu/Y, (f) 16Cu/Y_600 °C/20*h*/10% steam, (g) 16Cu/Y_700 °C/20*h*/10% steam and (h) 16Cu/Y_800 °C/20*h*/10% steam (Figure S2b). This material is available free of charge via the Internet at http://pubs.acs.org.

■ AUTHOR INFORMATION

Corresponding Author

*E-mail: andreas.martin@catalysis.de.

Notes

The authors declare no competing financial interest.

■ ACKNOWLEDGMENTS

This work is part of the MARTEC ERA-NET project (Project No. 03SX288A) funded by the Federal Ministry of Economy and Technology of Germany. The authors thank Dr. D.-L. Hoang for TPR, Dr. M. Schneider for XRD, Dr. J. Radnik for XPS, Mrs. A. Simmula for ICP-OES, and Mr. R. Eckelt for BET measurements.

■ REFERENCES

(1) Galloway, J. N.; Townsend, A. R.; Erisman, J. W.; Benkunda, M.; Cai, Z.; Freney, J. R.; Martinelli, L. A.; Seitzinger, S. P.; Sutton, M. A. *Science* **2008**, *320*, 889−892.

(2) Zhao, Y.; Duan, L.; Larssen, T.; Hu, L. H.; Hao, J. M. *Environ. Sci. Technol.* **2007**, *41*, 1815−1820.

(3) Granger, P.; Parvulescu, V. I. *Chem. Rev.* **2011**, *111*, 3155−3207.

(4) *International Convention for the Prevention of Pollution from Ships (MARPOL 73/78)*, appendix VI, 19.05;2005; pp 973−1978.

(5) Pietrzyk, P.; Gil, B.; Sojka, Z. *Catal. Today* **2007**, *126*, 103−111.

(6) Pietrzyk, P.; Zasada, F.; Piskorz, W.; Kotarba, A.; Sojka, Z. *Catal. Today* **2007**, *119*, 219−227.

(7) Ramprasad, R.; Hass, K. C.; Schneider, W. F.; Adams, J. B. *J. Phys. Chem. B* **1997**, *101*, 6903−6913.

(8) Ren, Y.; Harold, M. P. *ACS Catal.* **2011**, *1*, 969−988.

(9) Epling, W. S.; Campbell, L. E.; Yezerets, A.; Currier, N. W.; Parks, L. E. *Catal. Today* **2004**, *96*, 21−30.

(10) Epling, W. S.; Campbell, L.; Yezerets, A.; Currier, N. J. *Catal. Rev. Sci. Eng.* **2004**, *46*, 163−245.

(11) Abdulhamid, H.; Fridell, E.; Skoglundh, M. *Top. Catal.* **2004**, *30/31*, 161−168.

(12) Wu, Z.; Jin, R.; Liu, Y.; Wang, H. *Catal. Commun.* **2008**, *9*, 2217−2220.

(13) Liang, X.; Li, J.; Lin, Q.; Sun, K. *Catal. Commun.* **2007**, *8*, 1901−1904.

(14) Kustov, A. L.; Hansen, T. W.; Kustova, M.; Christensen, C. H. *Appl. Catal., B* **2007**, *76*, 311−319.

(15) Kobayashi, M.; Kuma, R.; Morita, A. *Catal. Lett.* **2006**, *112*, 37−44.

(16) Segura, Y.; Chmielarz, L.; Kustrowski, P.; Cool, P.; Dziembaj, R.; Vansant, E. F. *Appl. Catal., B* **2005**, *61*, 69−78.

(17) Seo, C.-K.; Choia, B.; Kima, H.; Leeb, C.-H.; Leeb, C.-B. *Chem. Eng. J.* **2012**, *191*, 331−340.

(18) Sobczak, I.; Musialska, K.; Pawlowski, H.; Ziolek, M. *Catal. Today* **2011**, *176*, 393−398.

(19) Rodríguez, G. C. M.; Saruhan, B.; Petrova, O.; Grünert, W. *Top. Catal.* **2009**, *52*, 1723−1727.

(20) Kumar, P. A.; Reddy, M.-P.; Lee, K.-J.; Phil, H.-H. *Catal. Lett.* **2008**, *126*, 78−83.

(21) Sparks, D. E.; Patterson, P. M.; Jacobs, G.; Dogimont, N.; Tackett, A.; Crocker, M. *Appl. Catal., B* **2006**, *65*, 44−54.

(22) Liu, Z. M.; Oh, K. S.; Woo, S. I. *Catal. Lett.* **2006**, *106*, 35−40.

(23) Li, J.; Hao, J.; Cui, X.; Fu, L. *Catal. Lett.* **2005**, *103*, 75−82.

(24) Jeon, J. Y.; Kim, H. Y.; Woo, S. I. *Appl. Catal., B* **2003**, *44*, 311−323.

(25) Zhang, F.; Zhang, S.; Guan, N.; Schreier, E.; Richter, M.; Eckelt, R.; Fricke, R. *Appl. Catal., B* **2007**, *73*, 209−219.

(26) Burch, R.; Breen, J. P.; Meunier, F. C. *Appl. Catal., B* **2002**, *39*, 283−303.

(27) Burch, R.; Breen, J. P.; Hill, C. J.; Krutzsch, B.; Konrad, B.; Jobson, E.; Cider, L.; Eranen, K.; Klingstedt, F.; Lindfors, L. E. *Top. Catal.* **2004**, *30/31*, 19−25.

(28) Parvulescu, V. I.; Granger, P.; Delmon, B. *Catal. Today* **1998**, *46*, 233−316.

(29) Ruette, F.; Sánchez, M.; Sierraalta, A.; Mendoza, C.; Añez, R.; Rodríguez, L.; Lisboa, O.; Daza, J.; Manrique, P.; Perdomo, Z.; Rosa-Brussin, M. *J. Mol. Catal. A* **2005**, *228*, 211−225.

(30) Schay, Z.; Guczi, L.; Beck, A.; Nagy, I.; Samuel, V.; Mirajkar, S. P.; Ramaswamy, A. B.; Pál-Borbèy, G. *Catal. Today* **2002**, *75*, 393−399.

(31) Sun, Q.; Sachtler, W. M. H. *Appl. Catal., B* **2003**, *42*, 393−401.

(32) Kubacka, A.; Janas, J.; Wloch, E.; Sulikowski, B. *Catal. Today* **2005**, *101*, 139−145.

(33) Shen, Q.; Li, L.; Hao, Z.; Xu, Z. *Appl. Catal., B* **2008**, *84*, 734−741.

(34) Chen, H. Y.; Wang, X.; Sachtler, W. M. H. *Appl. Catal., A* **2000**, *194/195*, 159−168.

(35) Iwamoto, M.; Hamada, H. *Catal. Today* **1991**, *10*, 57−61.

(36) Iwamoto, M.; Yahiro, H.; Tanda, K.; Mizuno, N.; Mine, Y.; Kagawa, S. *J. Phys. Chem.* **1991**, *95*, 3727−3730.

(37) Lombardo, E. A.; Sill, G. A.; d'Itri, J. L.; Hall, W. K. *J. Catal.* **1998**, *173*, 440−449.

(38) Desai, A. J.; Kovalchuk, V. I.; Lombardo, E. A.; d'Itri, J. L. *J. Catal.* **1999**, *184*, 396−405.

(39) Yahiro, H.; Iwamoto, M. *Appl. Catal., A* **2001**, *222*, 163−181.

(40) Amin, N. A. S.; Tan, E. F.; Manan, Z. A. *J. Catal.* **2004**, *222*, 100−106.

(41) Zhang, R.; Villanueva, A.; Alamdari, H.; Kaliaguine, S. *J. Catal.* **2006**, *237*, 368−380.

(42) Komvokis, V. G.; Iliopoulou, E. F.; Vasalos, I. A.; Triantafyllidis, K. S.; Marshall, C. L. *Appl. Catal., A* **2007**, *325*, 345−352.

(43) Lisi, L.; Pirone, R.; Russo, G.; Stanzione, V. *Chem. Eng. J.* **2009**, *154*, 341−347.

(44) Zhang, R.; Teoh, W. Y.; Amal, R.; Chen, B. H.; Kaliaguine, S. *J. Catal.* **2010**, *272*, 210−219.

(45) Erkfeldt, S.; Palmqvist, A.; Petersson, M. *Appl. Catal., B* **2011**, *102*, 547−554.

(46) Torre-Abreu, C.; Henriques, C.; Ribeiro, F. R.; Delahay, G.; Ribeiro, M. F. *Catal. Today* **1999**, *54*, 407−418.

(47) Kydd, R.; Teoh, W. Y.; Wong, K.; Wang, Y.; Scott, J.; Zeng, Q. H.; Yu, A. B.; Zou, J.; Amal, R. *Adv. Funct. Mater.* **2009**, *19*, 369−377.

(48) Carniti, P.; Gervasini, A.; Modica, V. H.; Ravasio, N. *Appl. Catal., B* **2000**, *28*, 175−185.

(49) Liu, Z.; Amiridis, M. D.; Chen, Y. *J. Phys. Chem. B* **2005**, *109*, 1251−1255.

(50) Chary, K. V. R.; Sagar, G. V.; Naresh, D.; Seela, K. K.; Sridhar, B. *J. Phys. Chem. B* **2005**, *109*, 9437−9444.

(51) Armor, J. N. *Appl. Catal., B* **1994**, *4*, N18−N19.

(52) Martec. http://www.martec-era.net/(accessed Jun 2, 2014).

(53) Schmidt, M.; Basner, R.; Brandenburg, R. *Int. J. Plasma Environ. Sci. Technol.* **2012**, *6*, 246−252.

(54) Schmidt, M.; Basner, R.; Brandenburg, R. *Plasma Chem. Plasma Proc.* **2013**, *33*, 323−335.

(55) Monti, D. A. M.; Baiker, A. *J. Catal.* **1983**, *83*, 323−335.

(56) Hoang, D.-L.; Lieske, H. *Thermochim. Acta* **2000**, *345*, 93−99.

(57) Gervasini, A.; Bennici, S. *Appl. Catal., A* **2005**, *281*, 199−205.

(58) Storck, S.; Bretinger, H.; Maier, W. F. *Appl. Catal., A* **1998**, *174*, 137−46.
(59) Hoang, D.-L.; Dang, T. T. H.; Engeldinger, J.; Schneider, M.; Radnik, J.; Richter, M.; Martin, A. *J. Solid State Chem.* **2011**, *184*, 1915−1923.
(60) Kieger, S.; Delahay, G.; Coq, B.; Neveu, B. *J. Catal.* **1999**, *183*, 267−280.
(61) Moreno-Tost, R.; Oliveira, M. L. M.; Eliche-Quesada, D.; Jimenéz-Jimenéz, J.; Jimenez-Lopes, A.; Rodriguez-Castellón, E. *Chemosphere* **2008**, *72*, 608−615.
(62) Moreno-Tost, R.; Santamaria-González, J.; Rodriguez-Castellón, E.; Jiménez-López, A.; Autié, M.; González, E.; De las Pozas, M. *Appl. Catal., B* **2004**, *50*, 279−288.
(63) Jolley, J. G.; Geesey, G.; Hawkins, M. R.; White, R. B.; Wichlacz, P. L. *Appl. Surf. Sci.* **1989**, *37*, 469−480.
(64) Mclynte, N. S.; Cook, M. G. *Anal. Chem.* **1975**, *47*, 2208−2213.
(65) Guczi, L.; Bazin, D. *Appl. Catal., A* **1999**, *188*, 163−174.
(66) Chusuei, C. C.; Brookshier, M. A.; Goodman, D. W. *Langmuir* **1999**, *15*, 2806−2808.
(67) Meda, L.; Cerofolini, G. F. *Surf. Interface Anal.* **2004**, *36*, 756−759.
(68) García-Cortés, J. M.; Pérez-Ramírez, J.; Rouzaud, J. N.; Vaccaro, A. R.; Illán-Gómez, M. J.; De Lecea, C.S.-M. *J. Catal.* **2003**, *218*, 111−122.
(69) Jen, H.-W. *Catal. Today* **1998**, *42*, 37−44.
(70) Iliopoulou, E. F.; Evdou, A. P.; Lemonidou, A. A.; Vasalos, I. A. *Appl. Catal., A* **2004**, *274*, 179−189.
(71) Lanza, R.; Eriksson, E.; Pettersson, L. J. *Catal. Today* **2009**, *147*, S279−S284.
(72) Cant, N. W.; Liu, I. O. Y. *Catal. Today* **2000**, *63*, 133−146.
(73) Matarrese, R.; Ingelsten, H. H.; Skoglundh, M. *J. Catal.* **2008**, *258*, 386−392.
(74) Metkar, P. S.; Balakotaiah, V.; Harold, M. P. *Catal. Today* **2012**, *184*, 115−128.
(75) Despres, J.; Koebel, M.; Kröcher, O.; Elsener, M.; Wokaun, A. *Microporous Mesoporous Mater.* **2003**, *58*, 175−183.
(76) Mulla, S. S.; Chen, N.; Cumaranatunge, L.; Delgass, W. N.; Epling, W. S.; Ribeiro, F. H. *Catal. Today* **2006**, *114*, 57−63.
(77) Bhatia, D.; McCabe, R. W.; Harold, M. P.; Balakotaiah, V. *J. Catal.* **2009**, *266*, 106−119.
(78) Kamasamudram, K.; Currier, N. W.; Chen, X.; Yezerets, A. *Catal. Today* **2010**, *151*, 212−222.